



Cite this: DOI: 10.1039/c6dt01180b

The interaction of Hg²⁺ and trivalent ions with two new fluorescein bio-inspired dual colorimetric/fluorimetric probes†

A. C. Gonçalves,^{a,b} V. Pilla,^{b,c} E. Oliveira,^b S. M. Santos,^d J. L. Capelo,^{b,e}
A. A. Dos Santos^{*a} and C. Lodeiro^{*b}

Two new luminescent compounds containing fluorescein–amino acid units have been designed and synthesized *via* an ester linkage between a fluorescein ethyl ester and Boc-Ser(TBDMS)-OH or Boc-Cys(4-MeBzl)-OH, and their photophysical properties have been explored. The optical response of both compounds (**2** and **3**) towards the metal ions Na⁺, K⁺, Hg⁺, Ag⁺, Ca²⁺, Co²⁺, Ni²⁺, Cu²⁺, Zn²⁺, Cd²⁺, Pb²⁺, Hg²⁺, Al³⁺, Fe³⁺, Ga³⁺ and Cr³⁺ was investigated in pure acetonitrile and in acetonitrile/water mixtures. A strong CHEF (Chelation-Enhanced Fluorescence) effect was observed with all the trivalent metals and Hg²⁺ ions in both solvents. UV-vis absorption, steady state and time resolved emission spectroscopy methods were employed. The results show the formation of mononuclear complexes with Al³⁺, Fe³⁺, Ga³⁺, Cr³⁺, and Hg²⁺. Theoretical calculation using Density Functional Theory was performed in order to obtain atomistic insights into the coordination geometry of Al³⁺ and Hg²⁺ to the fluorescein **3**, which is in accordance with the experimental stoichiometry results obtained in the Job's plot method. Among the active cations, the minimum detectable amount is under 1 μM for most of the cases in both absorption and fluorescence spectroscopy methods.

Received 26th March 2016,
Accepted 29th April 2016

DOI: 10.1039/c6dt01180b

www.rsc.org/dalton

Introduction

Fluorescein, and its derivatives, are a very interesting class of versatile green emissive dyes due to their potential application in biological fields such as in cellular biology, cellular imaging, as molecular tools in biochemistry and biomedical fields.^{1,2} Fluorescein-based derivatives are usually soluble in water, present good cell membrane penetration capacity, exhibit pH-responsive variations, show high fluorescence quantum yields, exhibit strong extinction coefficients, and are very useful for metal ion detection and quantification.^{3–7} In its free-acid form, fluorescein is a very versatile fluorogenic building block for organic synthesis, due to the presence of both

nucleophilic (phenolic) and electrophilic (carboxylate) functional groups. However, the presence of oxygenated functional groups around the whole of its molecular structure makes fluorescein poorly selective when seeking for a specific analyte or a class of analytes. The structural modification of the marginal functional groups of the xanthene moiety⁸ may allow the adjustment of the properties of the chromophore for specific applications making this dye one of the most widely explored probes. Having this concept in mind, the association of the fluorescein core with endogenous biomolecules such as amino acids or peptides^{9,10} is a promissory field of investigation since biocompatible chemosensors for *in vivo* applications can be envisioned. Metals like mercury (Hg²⁺) and chromium (Cr³⁺) are considered to be the most impactful with respect to their environmental contamination and toxicity to living organisms. Hg²⁺ exerts many toxic effects to living organisms including oxidative damage, neuro-toxicological disorders, carcinogenicity, *etc.*^{11,12} Mercury may occur in metallic, ionic, organometallic and complex forms,^{13,14} Hg²⁺ being the most stable oxidation state. In this form it can be easily bioaccumulated in foods or directly in animals, humans or other living entities.¹⁵ Hg²⁺ presents very high affinity for sulfur atoms, leading to very stable complexes; indeed, it is able to bind very efficiently to exogenous as well as endogenous sulfur-containing derivatives and this is the main reason for accumulative intoxication in living organisms.^{16,17} Concerning trivalent cations, Cr³⁺ is

^aInstituto de Química, Universidade de São Paulo, Av. Prof. Lineu Prestes, 748, CxP. 26077, São Paulo, 05508-000, Brazil. E-mail: alcindo@iq.usp.br

^bBIOSCOPE Group, UCIBIO-REQUIMTE, Departamento de Química, Faculdade de Ciências e Tecnologia, Universidade Nova de Lisboa, 2829-516 Portugal. E-mail: cle@fct.unl.pt, clodeiro@bioscopegroup.org

^cInstituto de Física, Universidade Federal de Uberlândia-UFU, Av. João Naves de Ávila 2121, Uberlândia, MG 38400-902, Brazil

^dCICECO - Aveiro Institute of Materials, Department of Chemistry, University of Aveiro, 3810-193 Aveiro, Portugal

^eProteomass Scientific Society, Rua dos Inventores, Madan Park, 2829-516 Caparica, Portugal

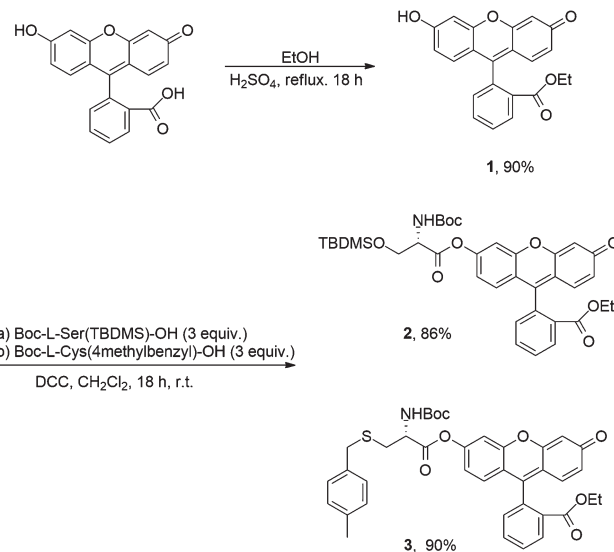
† Electronic supplementary information (ESI) available. See DOI: 10.1039/c6dt01180b

an essential element playing an important role in nutrition and some metabolic processes of humans but it is also a major environmental pollutant.^{18,19} The chromium oxidation states can range from -2 to $+6$, wherein Cr^{3+} is the far predominant species of chromium in living organisms.²⁰ Cr^{3+} plays essential roles in “trace amounts” (50–200 μg per day), necessary for the maintenance of glucose metabolism. However, the ingestion of doses up to 50 mg kg^{-1} is lethal in human adults.²¹ Al^{3+} is naturally abundant in silicates, cryolite and bauxite rocks, this last mineral being the main raw material in the production of metallic aluminum. It is even present in some pharmaceutical formulations as aluminum hydroxide in gastric pH regulators.²² Although not yet well understood, there is some evidence pointing to the association of Al^{3+} with brain disorders like Parkinson's and Alzheimer's disease.^{23,24} Considering the importance of these elements in life and consequently the need for their detection as well as quantification in different matrices, the development of selective and sensible analytical methods is still an interesting field of investigation.^{25–28} Xiaoxu Li *et al.*²⁹ demonstrated the construction of bio-inspired compounds by the union of amino acids and fluorescein from its phenolic group by a very simple strategy. Marta Mameli *et al.*¹¹ demonstrated the effect of the presence of the sulfur atom in anthracenylmethyl derivatives in order to design probes to detect Hg^{2+} . Barba-Bon *et al.*³⁰ reported the preparation of fluorescein ester derivatives used as probes for trivalent metallic ions. In order to apply accessible reagents as fluorescein and amino acids in the detection of metallic ions, in this work we present the synthesis, characterization and spectroscopic studies of two new fluorescein-based amino acid derivatives and their application for the fluorescence detection of some trivalent ions (Al^{3+} , Fe^{3+} , Ga^{3+} and Cr^{3+}) and Hg^{2+} . The molecular probe structures and their photophysical properties were characterized and their sensing ability towards a range of ions in acetonitrile and aqueous acetonitrile solutions was evaluated. DFT calculations were also performed to unveil the complexation mode by varying the metal ion.

Results and discussion

Synthetic approach

The first step of the synthetic route started with Fischer's esterification of fluorescein, followed by coupling with the amino acid derivatives Boc-ser(TMS)-OH and Boc-cys(4-methylbenzyl)-OH, using *N,N*-dicyclohexylcarbodiimide (DCC) as a carboxylic activator group, which resulted in the esters **2** and **3** in 86% and 90% yields, respectively as presented in Scheme 1. Both the compounds were characterized by ^1H and ^{13}C NMR, elemental analysis, mass spectrometry (MALDI-TOF-MS), UV-vis absorption, and emission spectroscopy, and lifetime measurements of the excited state were performed. The ^1H NMR spectra of **2** and **3** (Fig. S3 and S5†) present the singlet signal of the *t*-butyl from the *N*-Boc protective group and the characteristic signals of the amino acid backbone NH carbamate, $\alpha\text{-CH}$ and $\beta\text{-CH}_2$ from serine and cysteine side chains.



Scheme 1 Synthesis of ligands **2** and **3**.

For compound **2**, the *H*-methyl and *H*-*tert*-butyl attached to the silane group are observed in the upfield region of the spectra, due to the shielding effect by silicon.

Also, the signals due to the heterocyclic rings of the fluorescein moieties were visible between 6.5 and 8.3 ppm. The signals belonging to CH_2 (4.1 ppm) and CH_3 (1.0 ppm) from ethyl benzoate of fluorescein were observed for compounds **2** and **3**. Relative to the ^{13}C NMR spectra (Fig. S4 and S6†), the formation of the ester function was confirmed by the appearance of the signal of the quaternary carbonyl group at about 186 ppm, as well as by the α -carbon at 56.2 ppm (**2**) and 53.5 ppm (**3**). The IR spectra show some of the main signals, such as the carbonyl of the aliphatic ester that binds the fluorescein to the amino acid residue at 1770 cm^{-1} and the carbonyl of the ethyl benzoate at 1720 cm^{-1} . The broad band around 3300 cm^{-1} corresponds to the secondary N-H carbamate stretching present in both compounds **2** and **3**.³¹ Moreover, from the MALDI-TOF-MS analysis it is possible to identify the protonated molecular ion peak species [**2** + H^+] at 662.28 m/z and [**3** + H^+] at 668.23 m/z (Fig. S12 and S13†).

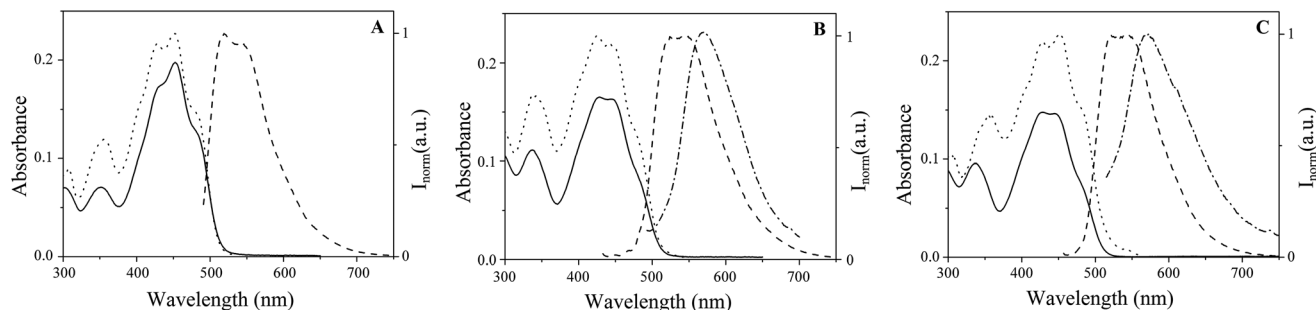
Photophysical characterization

The fluorescein derivatives **1**, **2** and **3** were characterized in acetonitrile at 298 K and the main characterization data were gathered and are given in Table 1. Fig. 1 presents the absorption, emission and excitation spectra of all compounds. Indeed, the perfect match between the absorption and excitation spectra rules out the absence of emissive impurities.

The absorption spectra revealed peaks at 452 nm for **1**, and 428 nm for **2** and **3** attributed to $\pi\text{-}\pi^*$ transitions of the fluorescein chromophore. Considering the emission spectra characteristic bands at 519 nm for **1** and 546 nm for **2** and **3** are visualized. The coupling of the amino-acids to compound **1** leads to a bathochromic shift of 24 and 27 nm in the absorption and emission maximum bands, and an increase in the

Table 1 UV-vis and fluorescence data for **1**, **2** and **3** (1×10^{-5} M) in acetonitrile

Compounds	UV-vis		Fluorescence				
	λ_{exc} (nm)	$\log \epsilon$	λ_{em} (nm)	λ_{em} Solid (nm)	Stokes' shift (nm)	Quantum yield ϕ	Lifetime τ (ns)
1	452	4.30	519	—	67	0.024	3.8 ± 0.1
2	428	4.22	546	576	118	0.002	2.3 ± 0.1
3	428	4.16	546	572	118	0.004	2.5 ± 0.1

**Fig. 1** Room temperature absorption (full line), normalized emission (dashed line, $\lambda_{\text{exc}} = 452$ nm in part A; $\lambda_{\text{exc}} = 428$ nm in parts B and C) and excitation spectra (dotted line, $\lambda_{\text{em}} = 519$ nm in part A; $\lambda_{\text{em}} = 546$ nm in parts B and C) of compounds **1** (A), **2** (B) and **3** (C) in acetonitrile (1.10^{-5} M). Emission spectra in the solid state (dotted dashed line, $\lambda_{\text{exc}} = 428$ nm, in parts B and C) of compounds **2** (B) and **3** (C).

Stokes' shift is also observed. The relative fluorescence quantum yields (Φ) of compounds **1** to **3** were calculated using acridine yellow as the standard ($\Phi = 0.47$ in ethanol),³² where values of 0.023, 0.002 and 0.004 were determined, respectively. As can be noted, the insertion of substituted amino acids in the precursor **1** at position 6 of the xanthene moiety led to a decrease of 10 times in the fluorescence quantum yield. In turn, when compared the quantum yield of **1** ($\Phi = 0.024$) with the free acid fluorescein in its neutral form ($\Phi = 0.30$),⁴ there was a decrease of 13 times in the emission of fluorescence. The decrease in the quantum yield of the free-acid fluorescein compared to **1** can be attributed to the steric hindrance imposed by the ethyl group, which results in a perpendicular arrangement between xanthene and benzoic moieties, making the π orbital overlap impaired, a condition for the π - π^* electronic transitions.³³ It is known that the methyl ester of fluorescein, where both hydroxyl groups are modified, is highly fluorescent.³³ However, herein two asymmetric probes (**2** and **3**) are reported, they can be compared with rhodols.³⁴ In the case of rhodols the fluorescence quantum yields decrease in accordance with the length of the linker. Fluorescence decays were measured in acetonitrile at 298 K, with excitation at 460 nm. All fluorescence decays were well fitted with a double exponential law, with decay times of 3.8, 2.3 and 2.5 ns, which are directly proportional to the quantum yield.³ The emission of compounds **2** and **3** was measured in the solid state using a fiber optic system connected to the HORIBA Scientific Fluoromax-4. In the solid state both compounds show the maximum emission peaks to be red shifted, $\Delta\lambda = 26$ – 30 nm, in relation to the ones obtained in solution, the maximum wavelength being located at 576 nm and 572 nm for compounds **2** and **3**, respectively.

Metallic ion sensing

The sensing ability of compounds **2** and **3** towards alkali (Na^+ , K^+), alkaline earth (Ca^{2+} , Ba^{2+}), transition (Co^{2+} , Ni^{2+} , Cu^{2+} , Fe^{3+} , Cr^{3+} , Ag^+ , Cd^{2+} , Hg^+ and Hg^{2+}), and post-transition (Zn^{2+} , Pb^{2+} , Al^{3+} , Ga^{3+}) metal ions were evaluated by ligand titrations with increasing additions of the metal salts. The titrations were followed by absorption and fluorescence emission spectroscopy. Both compounds were silent in the presence of alkaline and alkaline earth metal ions. Concerning transition and post-transition metal ions, only Hg^{2+} and the trivalent Fe^{3+} , Cr^{3+} , Al^{3+} and Ga^{3+} metal ions were able to coordinate with the fluorescein derivatives **2** and **3**. Fig. 2 shows the absorption and emission titrations of compounds **2** and **3** with the Hg^{2+} metal ion. A similar spectral behavior was observed in both compounds, whereas, in the absorption spectra, an increase at 431 nm and 434 nm in the absorbance with a concomitant disappearance of the band at 490 nm was detected, for compounds **2** and **3**, respectively. Probes **2** and **3** practically exhibit no fluorescence, however, surprisingly, a strong chelation-enhanced fluorescence (CHEF) at 470 nm (**2**) and 468 nm (**3**) was observed with Hg^{2+} . Due to its heavy metal ion nature, which usually leads to non-radiative decays, most systems using fluorescence spectroscopy for detecting Hg^{2+} are based on the complexation enhancement of the fluorescence quenching (CHEQ) effect.^{11,35–37} On the other hand, only a few fluorescence chemosensors are based on the CHEF effect.^{38–42}

Thus, this fact makes probes **2** and **3** very appealing for detection of toxic Hg^{2+} metal ions. Probes **2** and **3** also showed immediate turn-on upon the addition of trivalent metal ions,

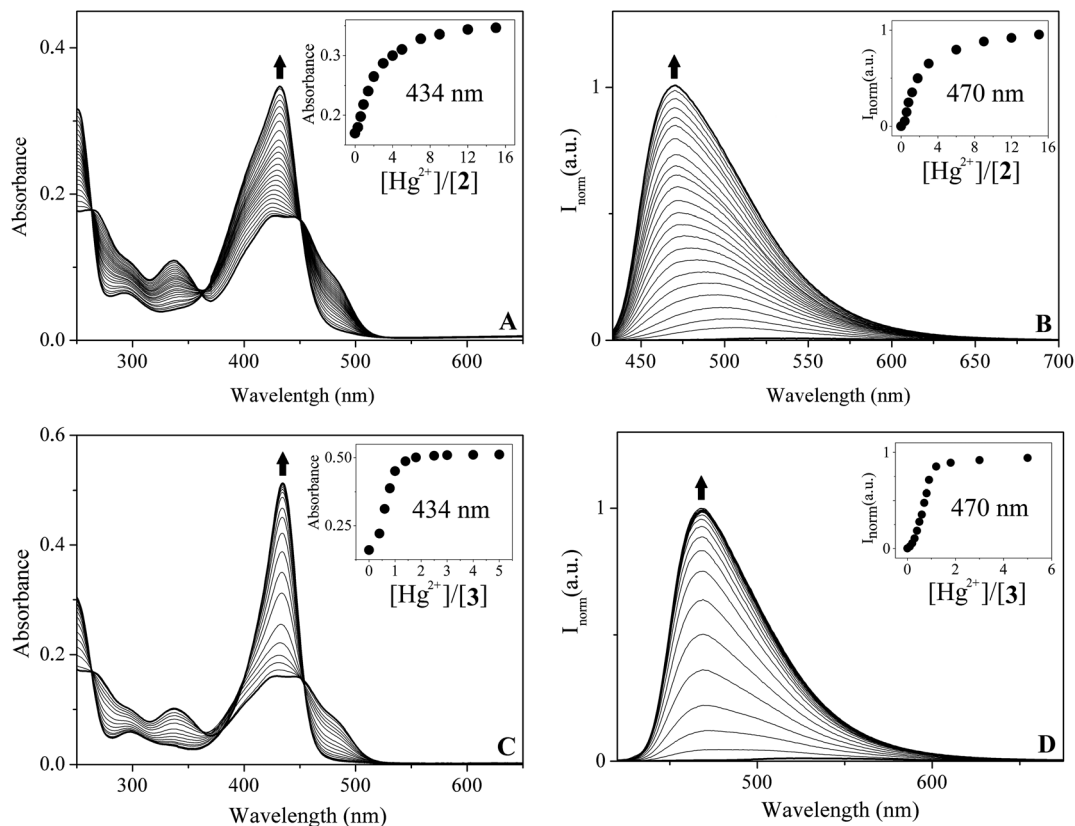


Fig. 2 Spectrophotometric titrations of **2** (A) and **3** (C), with increasing amounts of Hg^{2+} in acetonitrile solution. Inset: Absorption at 434 nm as a function of $[\text{Hg}^{2+}]/[\mathbf{2}]$ and $[\text{Hg}^{2+}]/[\mathbf{3}]$ ($T = 298 \text{ K}$; $[\mathbf{2}] = [\mathbf{3}] = 1.10^{-5} \text{ M}$). Spectrofluorometric titrations of **2** (B) and **3** (D), with increasing amounts of Hg^{2+} in acetonitrile solution. Inset: Emission at 470 nm as a function of $[\text{Hg}^{2+}]/[\mathbf{2}]$ and $[\text{Hg}^{2+}]/[\mathbf{3}]$ ($T = 298 \text{ K}$; $[\mathbf{2}] = [\mathbf{3}] = 1.10^{-5} \text{ M}$, $\lambda_{\text{exc}} = 362 \text{ nm}$).

such as Fe^{3+} , Cr^{3+} , Al^{3+} , and Ga^{3+} , despite Cr^{3+} and Fe^{3+} being known as fluorescence quenchers. Trivalent Cr^{3+} and Fe^{3+} are very effective fluorescence quenchers due to their paramagnetic nature, for this reason there are few turn-on sensors for these trivalent metal ions.^{43,44} In contrast Al^{3+} is diamagnetic, whereas its binding to sensors usually enhances the fluorescence signal. Fig. S7–S10[†] show the absorption and emission titration of both compounds with Al^{3+} , Fe^{3+} , Cr^{3+} and Ga^{3+} metal ions. Upon exposition of the probes to these metal ions, the absorbance at 490 nm decreases gradually and simultaneously a new significant band at 431 nm and 434 nm was developed. In the range of 450–600 nm, compounds **2** and **3** presented a weak emission, whereas a significant enhancement of the emission signal was detected at 500 nm and 493 nm for **2** and **3**, respectively. Barba-Bon and co-workers³⁰ published a similar selective turn-on chromo-fluorogenic probe for Fe^{3+} , Cr^{3+} and Al^{3+} , whereas they showed by NMR studies the eventual involvement of the xanthene moiety in the metal coordination. Atomistic insights into the coordination geometry of Al^{3+} and Hg^{2+} to the fluorescein **3** were obtained from density functional theory calculations with the B3LYP functional. The lowest energy complex conformations found for both 3-Al^{3+} and 3-Hg^{2+} (Fig. 3) involve the coordination of the metal to two carbonylic oxygens (from the ester moieties) and the sulphur from the thioether. In the case of 3-Al^{3+}

(Fig. 3A), the cation is tetrahedrally coordinated to the receptor ($d_{\text{Al}\dots\text{O}=\text{C}} = 1.77 \text{ \AA}$ and $d_{\text{Al}\dots\text{S}} = 2.30 \text{ \AA}$) and a water molecule ($d_{\text{Al}\dots\text{OH}_2} = 1.83 \text{ \AA}$). Similarly, and in the case of 3-Hg^{2+} (Fig. 3B), the cation is coordinated to the receptor ($d_{\text{Al}\dots\text{O}=\text{C}} = 2.45$ and 2.46 \AA and $d_{\text{Al}\dots\text{S}} = 2.74 \text{ \AA}$) and a water molecule ($d_{\text{Al}\dots\text{OH}_2} = 2.31 \text{ \AA}$) in a highly distorted tetrahedral geometry (the water molecule was included in the calculation as a way to provide an anchor point for stabilizing the coordination sphere of the cation).

On one hand, both binding arrangements suggest that the prearrangement of the two carbonyl groups and the thioether adequately provide a coordination pocket for accommodating the cation. On the other hand, the ionic radius of the metallic cation suggests that it plays an important role in the overall conformation of the association since coordination to larger cations can lead to the involvement of the ester oxygens from the fluorescein moiety. These results support the experimentally inferred coordination mode of the metal to the receptor. The association constants using the HypSpec⁴⁵ program corroborate the theoretical model complexation of one ligand per metal ion ($L : M 1 : 1$), and the main results are summarized in Table 2.

The values obtained are almost of the same order ($\log \beta \approx 5$), with the exception of Hg^{2+} whereas a higher value of $\log \beta \approx 6.5$ was observed for compound **3**. This fact is due to the presence of the sulphur atom in the cysteine amino acid in

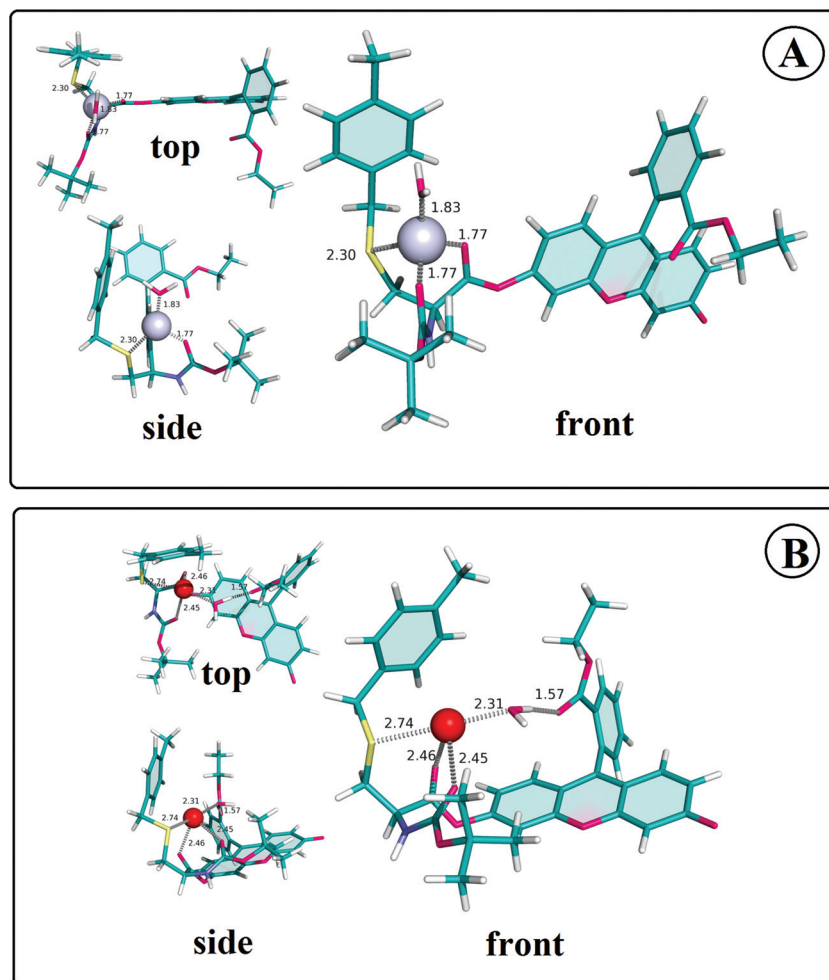


Fig. 3 (A) Top, side and front views of the lowest energy conformation of the **3**–Al³⁺ complex, indicating the distances between the receptor's interaction sites and cation (color code: C – teal; O – pink; H – white; S – yellow; N – blue, Al – light blue sphere). (B) Top, side and front views of the lowest energy conformation of the **3**–Hg²⁺ complex, indicating the distances between the receptor's interaction sites and cation (color code as in (A); Hg – red sphere).

Table 2 Stability constants $\log \beta$ obtained from absorbance (A) and fluorescence (F) titration data. The HypSpec program was applied considering 1 : 1 interaction

Compounds	2		3	
	$\log \beta$ (A)	$\log \beta$ (F)	$\log \beta$ (A)	$\log \beta$ (F)
Hg ²⁺	5.1 ± 0.1	5.4 ± 0.1	6.5 ± 0.2	6.2 ± 0.2
Ga ³⁺	5.0 ± 0.2	4.8 ± 0.3	5.4 ± 0.3	5.8 ± 0.3
Cr ³⁺	5.2 ± 0.3	4.9 ± 0.2	5.3 ± 0.1	5.1 ± 0.3
Al ³⁺	5.3 ± 0.3	5.1 ± 0.3	5.5 ± 0.1	5.1 ± 0.3
Fe ³⁺	5.0 ± 0.3	5.2 ± 0.2	4.9 ± 0.3	5.5 ± 0.1

compound **3**, which confers a higher affinity to the Hg²⁺ metal ion.⁴⁶ The final stoichiometry of **2** and **3** with each of the ions was confirmed by the Job's plot method and the results are compiled in Fig. S14.† Fig. 4 shows a general overview of the fluorescence properties of the probes **2** and **3** upon the addition of all the metal ions studied. The emission spectra of **2** and **3** upon the addition of 4 equivalents of alkali (Na⁺, K⁺),

alkaline earth (Ca²⁺, Ba²⁺), transition (Co²⁺, Cu²⁺, Ni²⁺, Ag⁺, Cd²⁺, Hg⁺, Hg²⁺, Fe³⁺, Cr³⁺) and post-transition (Zn²⁺, Pb²⁺, Al³⁺, Ga³⁺) metal ions were recorded. Careful inspection of Fig. 4 leads to the conclusion that **2** and **3** show a turn-on and an unprecedented selectivity for Hg²⁺, Al³⁺, Fe³⁺, Cr³⁺ and Ga³⁺ metal ions producing intense emissive green-blue colours upon complexation by these metals. The difference in the coordination mode observed in the DFT calculations can be extended to the other trivalent ion complexes, and is reflected directly in the emission wavelengths: green for X³⁺ (around 500 nm) and blue for Hg²⁺ (470 nm), as shown at the bottom of Fig. 4B. In order to study the properties of probes **1**, **2** and **3**, the photophysical characterization in a mixture of acetonitrile/water (1 : 1) was carried out (Fig. 5). The addition of water induces a red shift in the maximum of absorption, from 428 nm to 460 nm in compounds **2** and **3**.

As is known, due to the high affinity of the studied metallic ions for water, the addition of an excess of water to the system involving the probes/analytes in acetonitrile solution induces

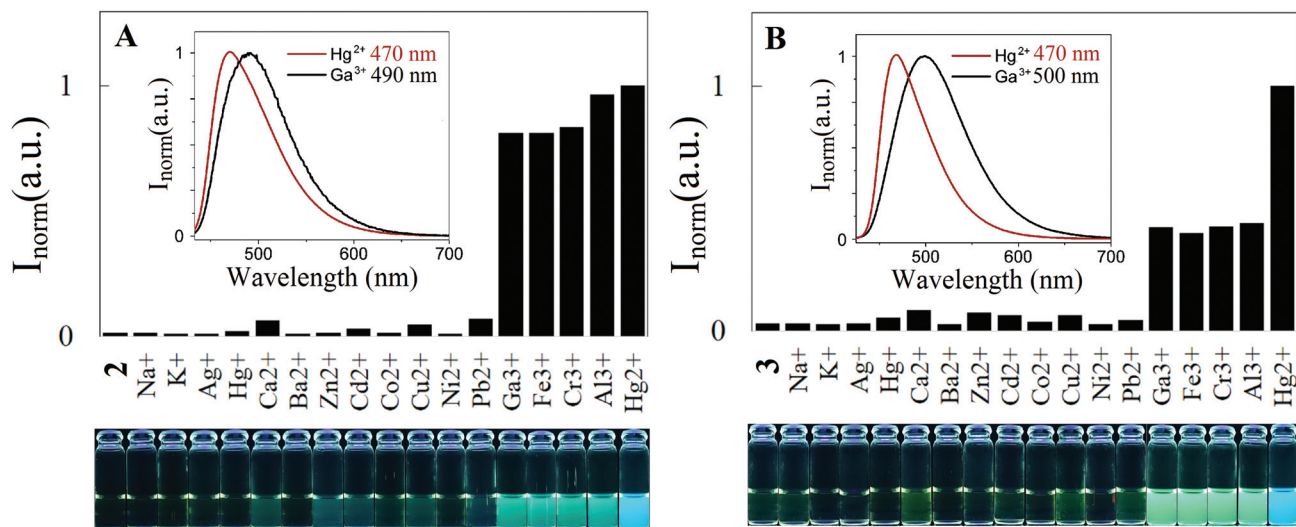


Fig. 4 Relative emission intensity of **2** (A) and **3** (B) upon addition of 4 equiv. of Na^+ , K^+ , Ca^{2+} , Ba^{2+} , Zn^{2+} , Co^{2+} , Cu^{2+} , Ni^{2+} , Ag^+ , Cd^{2+} , Hg^+ , Hg^{2+} , Fe^{3+} , Cr^{3+} , Al^{3+} , Ga^{3+} and Pb^{2+} in acetonitrile ($[\text{A}] = [\text{B}] = 1 \times 10^{-5} \text{ M}$; $\lambda_{\text{exc}} = 362 \text{ nm}$). Inset: Normalized emission displacement between the complexes of Hg^{2+} and Ga^{3+} for **2** (A) and **3** (C). Bottom: Visual changes of **2** (left) and **3** (right) under UV light after addition of metallic ions ($\lambda_{\text{exc}} = 365 \text{ nm}$).

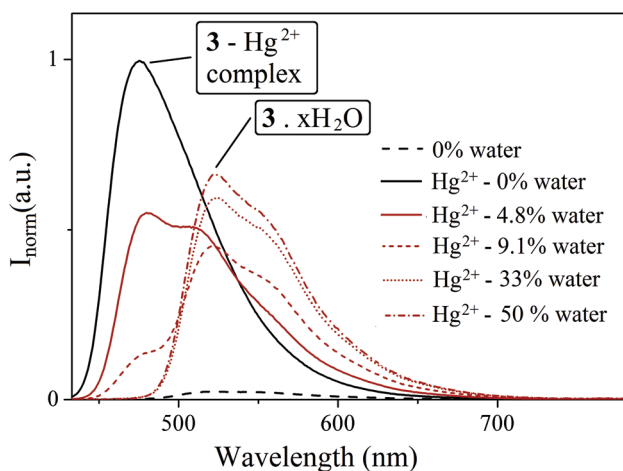


Fig. 5 Progress of emission spectra of the complex **3**- Hg^{2+} (4 equiv.) in solutions with different amounts of water in acetonitrile ($[\text{3}] = 1 \times 10^{-5} \text{ M}$; $\lambda_{\text{exc}} = 423 \text{ nm}$).

quenching of the fluorescence emission, due to that the coordination sphere of the ions is substituted by water molecules. The presence of water in the metal complex **3**- Hg^{2+} was studied by fluorescence analysis in different percentages of water (4.8%, 9.1%, 33% and 50%) in acetonitrile. The emission band at 470 nm (black solid line), related to complex **3**- Hg^{2+} is completely quenched up to 9.1% of water. Up to 4.8% of water, the main emission band is not that observed for the complex **3**- Hg^{2+} at 470 nm, but at 525 nm, which belongs to the species between compound **3** bounded to water molecules through hydrogen bonds, as shown in Fig. S15.†

In order to shed more light on the sensing ability of these systems, the minimal detectable and quantified amount of

Table 3 Minimal detectable and quantified amount (μM) for Hg^{2+} , Fe^{3+} , Cr^{3+} , Al^{3+} and Ga^{3+} metal ions in acetonitrile. Relative standard deviation (RSD) of the values measured was below 10%, $n = 3$

Compounds	Metal ions	Minimal detectable amount (μM)		Minimal quantified amount (μM)	
		Abs	Em	Abs	Em
2	Hg^{2+}	1.04	9.76	1.15	26.7
	Fe^{3+}	0.99	0.28	1.10	0.76
	Cr^{3+}	1.08	0.23	1.18	0.64
	Al^{3+}	0.95	0.20	1.05	0.55
	Ga^{3+}	1.09	0.34	1.20	0.93
3	Hg^{2+}	0.97	0.86	1.07	1.43
	Fe^{3+}	0.91	0.40	1.00	0.67
	Cr^{3+}	0.88	0.24	0.97	0.40
	Al^{3+}	0.82	0.22	0.91	0.37
	Ga^{3+}	0.99	0.31	1.10	0.52

Hg^{2+} , Fe^{3+} , Cr^{3+} , Al^{3+} and Ga^{3+} was determined according to the procedure described in the Experimental section. The resulting values were gathered and are given in Table 3. The limit of detection by absorption for compounds **2** and **3** was obtained applying eq. (1), $\text{LOD}_{\text{abs}} = 0.16 \pm 0.01$; and by emission the results are $\text{LOD}_{\text{em}2} = 0.04 \pm 0.01$ and $\text{LOD}_{\text{em}3} = 0.16 \pm 0.01$. Regarding the limit of quantification using eq. (2), the $\text{LOQ}_{\text{abs}} = 0.18 \pm 0.02$ for both compounds and $\text{LOQ}_{\text{em}2} = 0.10 \pm 0.03$, and $\text{LOQ}_{\text{em}3} = 0.18 \pm 0.02$ were obtained by absorption and emission, respectively. The minimal detectable amount obtained by absorption for the metal ions studied ranges from 0.95–1.09 μM and 0.88–0.99 μM for compounds **2** and **3**, respectively. Through emission spectra, the value ranges between 0.20–9.76 μM (**2**) and 0.31–0.86 μM (**3**) were determined.

It is clearly notable that compound **3** is more sensitive and reactive to the metal ions studied than **2**, showing lower detectable amounts. This fact is evident for Hg^{2+} metal ions, whereas a remarkable decrease from 9.76 to 0.97 μM (10 times) in the detectable amount was determined (Table 3). Once more, this is attributed to the presence of the amino acid cysteine, which contains a sulphur atom with high affinity to this heavy metal ion.⁴⁶ Regarding the minimal quantified amount for Hg^{2+} , Fe^{3+} , Cr^{3+} , Al^{3+} and Ga^{3+} metal ions in acetonitrile, the values between 0.91 and 1.20 μM were calculated by absorption; 0.55–26.7 μM for **2** and 0.52–1.43 μM for **3** were calculated by emission. This clearly makes compound **3** the best probe to be used as an analytical tool for trivalent and Hg^{2+} metal ion detection. Our systems show similar detection results to the one published previously by Barba-Bon and co-workers.³⁰ However for Cr^{3+} ions our probes showed to be more effective since the detectable amounts by absorption and emission are lower. In our systems, the lowest values of 0.88 μM and 0.23 μM are determined respectively, by absorp-

tion and emission, in comparison with the amounts of 2.5 and 0.5 μM published previously.³⁰

Lifetime and fluorescence quantum yield of the metal complexes

Fluorescence decays of the ligands and complexes were measured in acetonitrile. The main data are depicted in Table 4. As a representative example, Fig. 6A shows the fluorescence decay of the **2**- Hg^{2+} complex and also the correlation between the lifetime and quantum yield of **2**, **3** and the complexes (Fig. 6B and C). The fluorescence decays of both compounds and their metallic complexes were fitted with a double exponential law, suggesting two different conformers in the excited state.^{33,47} However, in the case of the free ligands, the relative amplitudes (B ~ 3% and C ~ 97%, Table 4) indicate a predominant species in solution of a short lifetime and low quantum yield. On the other hand, by the analysis of the complexes, the higher values of amplitudes follow the higher lifetimes, indicating an effective complex formation. These

Table 4 Fluorescence quantum yield and lifetime for compounds **2** and **3**. Fluorescence decays for **2** and **3** were fitted using $A + B \text{Exp}(-t/\tau) + C \text{Exp}(-t/\tau^*)$. The values presented are average of six independent measurements

Compounds	2			3		
	ϕ	τ	τ^*	ϕ	τ	τ^*
		(ns)			(ns)	
		B [Rel. amp. %]	C		B [Rel. amp. %]	C
Free ligand	0.002 ± 0.001	2.3 [2.9]	0.13 [97.1]	0.005 ± 0.001	2.5 [4.1]	0.37 [95.9]
Hg^{2+}	0.14 ± 0.01	3.9 [96]	0.5 [4]	0.16 ± 0.01	3.4 [91]	0.6 [9]
Fe^{3+}	0.11 ± 0.01	3.8 [44]	0.06 [56]	0.12 ± 0.02	3.2 [50]	0.10 [50]
Al^{3+}	0.11 ± 0.01	3.8 [79]	0.11 [21]	0.12 ± 0.03	3.2 [70]	0.24 [30]
Cr^{3+}	0.12 ± 0.01	3.8 [5.4]	0.072 [46]	0.12 ± 0.02	3.1 [60]	0.13 [40]
Ga^{3+}	0.12 ± 0.01	3.8 [80]	0.09 [20]	0.12 ± 0.02	3.2 [80]	0.31 [20]

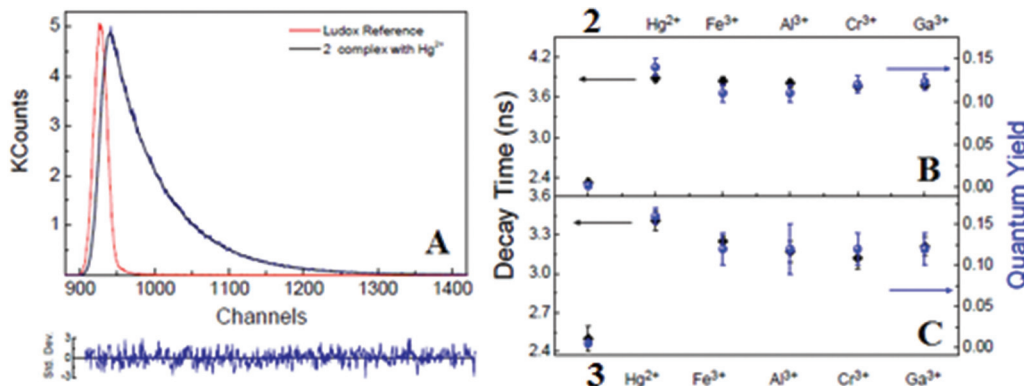


Fig. 6 (A) Fluorescence decays and global analysis of **2** (Flu-TMS) with 4 equivalents of Hg^{2+} and the Ludox reference. The decay time values obtained for fitting with a sum of two exponentials are 0.49 and 3.87 ns, Chisq 1.06. Decay time and quantum yield averages for (B) **2** and (C) **3** complexes are presented.

results are in accordance with the literature, where multiple (with two lifetimes of ~ 4 ns and ~ 0.5 – 2 ns) and single decays have been reported to ligand coupled fluorescein structures.⁴⁷ The insertion of amino acid derivatives at the backbone of the xanthene unit in the precursor **1** leads to a decrease in the fluorescence quantum yield from $\phi_1 = 0.024 \pm 0.001$ to $\phi_2 = 0.002 \pm 0.001$ and $\phi_3 = 0.005 \pm 0.001$ (*ca.* 10-times lower). However, upon complexation a strong CHEF takes place, resulting in values of fluorescence quantum yield between 0.11 and 0.16, which represents a huge increase ranging from 24 to 70 times, compared to the free ligands. The same behavior was observed in lifetime measurements, whereas higher values were obtained for the metal complexes ($\tau = 3.1$ – 3.9 ns) in comparison with the free ligands ($\tau = 2.3$ – 2.5 ns).

The lifetime values obtained showed no significant difference between compounds **2** and **3**. These results are in agreement with the ones obtained for the fluorescence quantum yield, once generally, emissive systems with higher fluorescence quantum yields are more stable in the excited state.

Conclusions

Two new bio-inspired fluorescein derivatives were successfully synthesized and applied as probes for Hg^{2+} and trivalent metallic ions in acetonitrile solution. The complexation process promoted huge changes in the photophysical properties of free ligands. A strong CHEF, an absorption blue shift, an increase in extinction coefficient, longer lifetimes of the excited states and higher quantum yields of fluorescence were observed as result of the complex formation. DFT calculations suggested different models of interaction between the **3**– Al^{3+} and **3**– Hg^{2+} complexes, which were reflected in the green emission of the trivalent ion complexes and blue emission of the Hg^{2+} complex. The application of compounds **2** and **3** as analytical probes for Al^{3+} sensing reached the lowest detection and quantification limits in both absorption and fluorescence techniques, compared to other metals. The interaction constants of the complexes all showed very close values, except for **3**– Hg^{2+} , which presented considerably higher values attributed to the soft–soft attraction between Hg^{2+} and S-cysteine, reinforcing the Pearson's acid–base concept. This result suggests the importance of the sulfur atom in the amino acid residue to modulate the metal–ligand interaction constants for soft metal ions. As the presence of water suppresses the sensing ability of the probes, these are very promising structures to be applied in the selective detection of the studied cations in biological aprotic environments, such as cell membranes or micellar systems. These further studies are under investigation in our group.

Experimental section

Chemicals and starting materials

The fluorescein (free acid) was purchased from Fluka, Boc-Cys-(4-MeBzl)-OH and metallic salts ($\text{Hg}(\text{ClO}_4)_2 \cdot 3\text{H}_2\text{O}$, $\text{Al}(\text{NO}_3)_3 \cdot$

$9\text{H}_2\text{O}$, $\text{Cr}(\text{NO}_3)_3 \cdot 9\text{H}_2\text{O}$, $\text{Fe}(\text{NO}_3)_3 \cdot 9\text{H}_2\text{O}$, $\text{Ga}(\text{NO}_3)_3 \cdot 9\text{H}_2\text{O}$, $\text{Zn}(\text{NO}_3)_2 \cdot 6\text{H}_2\text{O}$, $\text{Ca}(\text{BF}_4)_2 \cdot x\text{H}_2\text{O}$, $\text{Cd}(\text{ClO}_4)_2 \cdot 6\text{H}_2\text{O}$, $\text{Co}(\text{NO}_3)_2 \cdot 6\text{H}_2\text{O}$, $\text{Ni}(\text{NO}_3)_2 \cdot 6\text{H}_2\text{O}$, $\text{Cu}(\text{NO}_3)_2 \cdot 6\text{H}_2\text{O}$, $\text{Pb}(\text{ClO}_4)_2 \cdot 3\text{H}_2\text{O}$, $\text{Hg}(\text{ClO}_4)_2 \cdot 4\text{H}_2\text{O}$, NaNO_3 , KNO_3 , AgNO_3) were purchased from Sigma-Aldrich and used as received. Boc-Ser(TBDMS)-OH was prepared as reported in the literature.⁴⁸

Instruments

Elemental analysis was performed using a Thermo-Finnigan CE Flash-EA 1112-CHNS instrument provided by the Chemical Analysis Service of the REQUIMTE, DQ, Universidade Nova de Lisboa, Monte da Caparica, Portugal. Mass spectrometry characterization of compounds **1** and **2** was carried out in an Ultraflex II MALDI-TOF/TOF instrument from Bruker Daltonics (BIOSCOPE-PROTEOMASS Research Lab) and high-resolution mass spectrometry spectrum of compound **3** was recorded in an Electron Spray Ionization Time of Flight (ESI-TOF) microTOF-QII Bruker spectrometer (IQ-Universidade de São Paulo). ^1H and ^{13}C NMR spectra were recorded on a Bruker Avance III 200 (200 MHz, ^1H ; 50 MHz, ^{13}C) spectrometer at Universidade de São Paulo, São Paulo, Brazil. The lifetime of the excited state was measured using a Horiba Jobin-Yvon Temprom equipped with the light source NanoLED at 460 nm, PROTEOMASS Scientific Society, Portugal. The infra-red spectra were recorded on a Spectrum BX Perkin-Elmer FT-IR System.

Spectrophotometric and spectrofluorometric measurements

Absorption spectra were recorded on a Jasco V-650 spectrophotometer and fluorescence emission on a Horiba-Yvon-Spex Fluoromax-4 spectrofluorometer. A correction for the absorbed light was applied when necessary. All spectrofluorometric titrations were performed as follows: the stock solutions of the ligands (*ca.* 5×10^{-4} M) were prepared by dissolving an appropriate amount of the ligands in 25 mL volumetric flasks to the mark with acetonitrile. The titration solutions were prepared by dilution of stock solutions at a final concentration of 1×10^{-5} M in acetonitrile. Titrations of the ligands were conducted by the addition of microliters of standardized metal solutions in acetonitrile. The absorption and emission spectra of these solutions were recorded after additions ($\lambda_{\text{exc}} = 428$ nm and $\lambda_{\text{em}} = 546$ nm for **2** and **3**). The stock solutions of the metallic ions were prepared by dissolving an appropriate amount of the salts in 10 mL volumetric flasks to the mark with water (*ca.* 0.05 M). The titration solutions of metals were obtained by the dilution of the stock solution to the concentration of 1.5×10^{-3} M in acetonitrile. The solid-state emission spectra of **2** and **3** were recorded on a Horiba-Scientific Fluoromax-4 spectrofluorometer using an external fiber-optic device. The fluorescence quantum yield of compounds **1**, **2** and **3** was measured using a solution of acridine yellow in absolute ethanol as the standard ($\phi = 0.47$)⁴⁹ and was corrected for different refraction indexes of solvents. The detection (LOD) and quantification (LOQ) limits for the metal ions were determined, having in mind their use for real metal ion detection and for analytical applications. For these measurements, ten

different analyses for the selected receptor were performed in order to obtain the LOD and LOQ.

The LOD and LOQ were obtained by applying the equations:

$$\text{LOD} = y_{\text{blank}} + 3 \text{ std} \quad (1)$$

$$\text{LOQ} = y_{\text{blank}} + 10 \text{ std}; \quad (2)$$

where y_{blank} = signal detection limit and std = standard deviation.

Theoretical calculations

All calculations were performed with Gaussian09 (19) using Density Functional Theory with the B3LYP functional and the 6-31G** (C, H, N, O, S, Al) and LanL2DZ (Hg) basis set, as implemented in Gaussian09. Default optimization parameters were used throughout the calculations.

Synthesis of organic compounds

Synthesis of 2-(6-hydroxy-3-oxo-3H-xanthen-9-yl)benzoate (1). In a 500 mL round bottomed flask, concentrated sulfuric acid (15 mL) was added dropwise to a solution of fluorescein (30.09 mmol, 10 g) in ethanol (200 mL) at room temperature. After stirring and refluxing for 18 hours, the solvent was removed in a rotatory evaporator and the resulting mixture was diluted in chloroform and transferred to a 1000 mL beaker. Solid sodium bicarbonate was added to the mixture until evolution of carbon dioxide ceased. The heterogeneous mixture was filtered through a Buchner funnel and the organic phase was evaporated. The crude product was dissolved in 400 mL of ethanol (96%) at boiling temperature. The volume was reduced to 100 mL by boiling and the resulting solution was allowed to stand for 12 hours at $-20\text{ }^{\circ}\text{C}$, yielding 8.90 g of pure product as brown crystals, with a greenish glow. Yield 90%. Melting point: $242\text{ }^{\circ}\text{C}$. $^1\text{H NMR}$ (200 MHz, DMSO) δ 8.18 (d, $J = 7.4$ Hz, 1H), 8.00–7.61 (m, 2H), 7.50 (d, $J = 7.0$ Hz, 1H), 6.80 (d, $J = 9.6$ Hz, 2H), 6.56 (d, $J = 6.6$ Hz, 4H), 3.96 (q, $J = 7.0$ Hz, 2H), 0.86 (t, $J = 7.1$ Hz, 3H). $^{13}\text{C NMR}$ (50 MHz, DMSO) δ 173.93, 165.02, 156.13, 150.49, 133.66, 132.91, 130.61, 130.06, 129.87, 121.75, 114.39, 103.24, 60.83, 13.29. UV-vis in acetonitrile; λ_{max} , nm (ϵ_{max} , $\text{dm}^3 \text{ mol}^{-1} \text{ cm}^{-1}$): 452 (19 953). Fluorescence emission in acetonitrile ($\lambda_{\text{exc}} = 452$ nm, $\lambda_{\text{em}} = 519$ nm).

Synthesis of (S)-ethyl 2-(6-((2-((tert-butoxycarbonyl)amino)-3-((tert-butyl)dimethylsilyl)oxy)propanoyl)oxy)-3-oxo-3H-xanthen-9-yl)benzoate (2). In a round bottomed flask of 50 mL under an inert atmosphere, Boc-Ser(TBDMS)-OH (3.0 mmol, 1.05 g); *N,N'*-dicyclohexylcarbodiimide (DCC, 3 mmol, 0.6 mL) and dichloromethane (20 mL) were added while stirring for 15 minutes. Subsequently, **1** was added (1.1 mmol, 0.386 g) and the reaction was followed until all the fluorescein derivative was consumed. After 18 hours, the reaction medium was filtered to remove the urea generated by the consumption of DCC, and the solvent was removed under reduced pressure in a rotatory evaporator. The product was purified in a chromatographic column using flash silica as the stationary phase and an ethyl acetate/hexane mixture in the ratio 2:1 as the

eluent. The pure product was obtained as an orange solid in 86% yield.

RF in EtOAc/hexane 2:1 = 0.50. Melting point: $68\text{ }^{\circ}\text{C}$. Elemental analysis (found: C, 65.1; H, 6.7; N, 2.2% CHNS requires: C, 65.3; H, 6.6; N, 2.1) $^1\text{H NMR}$ (200 MHz, CDCl_3) δ 8.36–8.20 (m, 1H), 7.72 (td, $J = 6.7, 1.6$ Hz, 2H), 7.42–7.28 (m, 1H), 7.08–6.80 (m, 3H), 6.64–6.40 (m, 2H), 5.41 (d, $J = 8.7$ Hz, 1H), 4.62 (d, $J = 8.7$ Hz, 1H), 4.33–3.83 (m, 4H), 1.48 (s, 9H), 0.98 (t, $J = 7.1$ Hz, 3H), 0.90 (d, $J = 0.8$ Hz, 9H), 0.16–0.02 (m, 6H). $^{13}\text{C NMR}$ (50 MHz, CDCl_3) δ 186.19, 169.19, 165.41, 158.74, 155.65, 154.09, 152.90, 149.16, 134.07, 132.94, 131.60, 130.99, 130.90, 130.68, 130.57, 130.07, 128.91, 119.95, 119.42, 118.22, 110.23, 106.46, 80.61, 63.95, 61.69, 56.18, 28.52, 25.98, 18.45, 13.78, 0.20, -5.28 . MALDI-TOF-MS [calcd (found)]: 662.28 (662.28) [M + H]. UV-vis [acetonitrile; λ_{max} , nm (ϵ_{max} , $\text{dm}^3 \text{ mol}^{-1} \text{ cm}^{-1}$): 337 (10 727), 428 (16 019), 444 (15 835). Fluorescence emission in acetonitrile ($\lambda_{\text{exc}} = 428$ nm, $\lambda_{\text{em}} = 546$ nm). IR (BaF₂ windows, cm^{-1}): 2954, 2933, 2859, 1774, 1717, 1645, 1598, 1523, 1367, 1259, 1153, 1106, 838, 777.

Synthesis of (R)-ethyl 2-(6-((2-((tert-butoxycarbonyl)amino)-3-((4-methylbenzyl)thio)propanoyl)oxy)-3-oxo-3H-xanthen-9-yl)benzoate (3). The same procedure was performed as for obtaining **2**, replacing Boc-Ser(TBDMS)-OH by Boc-Cys(4methylbenzyl)-OH. The pure product was obtained as an orange solid in 90% yield. RF in EtOAc/hexane 2:1 = 0.54. Melting point: $66\text{ }^{\circ}\text{C}$. Elemental analysis (found: C, 68.1; H, 5.7; N, 2.1; S, 4.7% CHNS requires: C, 68.4; H, 5.6; N, 2.1; S, 4.8). $^1\text{H NMR}$ (200 MHz, CDCl_3) δ 8.43–8.17 (m, 3H), 7.92–7.55 (m, 6H), 7.04 (ddd, $J = 19.0, 15.8, 12.5$ Hz, 28H), 6.69–6.41 (m, 4H), 5.33 (d, $J = 7.6$ Hz, 3H), 4.74 (d, $J = 7.6$ Hz, 4H), 4.06 (q, $J = 7.1$ Hz, 7H), 3.77 (s, 5H), 2.98 (d, $J = 5.4$ Hz, 5H), 2.33 (s, 9H), 1.47 (s, 30H), 0.99 (t, $J = 7.1$ Hz, 8H). $^{13}\text{C NMR}$ (50 MHz, CDCl_3) δ 186.01, 172.95, 169.19, 165.09, 158.64, 157.50, 155.13, 153.74, 152.64, 149.54, 137.09, 134.15, 133.75, 132.70, 131.35, 130.59, 130.47, 130.38, 129.89, 129.74, 129.36, 129.14, 128.79, 121.87, 119.63, 119.26, 118.10, 115.21, 110.06, 106.08, 103.81, 80.59, 61.45, 53.49, 36.39, 33.11, 28.24, 21.06, 13.57. MALDI-TOF-MS [calcd (found)]: 668.23 (668.23) [M + H]. UV-vis [acetonitrile; λ_{max} , nm (ϵ_{max} , $\text{dm}^3 \text{ mol}^{-1} \text{ cm}^{-1}$): 336 (9360), 428 (14 425), 445 (14 350). Fluorescence emission in acetonitrile ($\lambda_{\text{exc}} = 428$ nm, $\lambda_{\text{em}} = 546$ nm). IR (BaF₂ windows, cm^{-1}): 2974, 2918, 1771, 1715, 1639, 1598, 1509, 1263, 1158, 860.

Acknowledgements

E. Oliveira acknowledges the post-doctoral grant from Fundação para a Ciência e a Tecnologia (FCT-MEC) (Portugal) SFRH/BPD/72557/2010. A. Gonçalves and V. Pilla thank CNPq/Brazil for the PhD and post-doctoral (202553/2014-0) grant respectively. C. Lodeiro thanks the CNPq program, Science without borders 2014–2016 grant (Brazil). Financial support from the Scientific PROTEOMASS Association (Portugal), the University of São Paulo through the NAP-CatSinQ (Research Core in Catalysis and Chemical Synthesis), FAPESP, CAPES and FAPEMIG (Brazil) (APQ-00360-14) is acknowledged. This work

was supported by the Unidade de Ciências Biomoleculares Aplicadas-UCIBIO which is financed by national funds from FCT/MEC (UID/Multi/04378/2013) and co-financed by the ERDF under the PT2020 Partnership Agreement (POCI-01-0145-FEDER-007728). Part of this work was developed within the scope of the project CICECO-Aveiro Institute of Materials, POCI-01-0145-FEDER-007679 (FCT Ref. UID/CTM/50011/2013), financed by national funds through the FCT/MEC and when appropriate co-financed by FEDER under the PT2020 Partnership Agreement. S. M. S. thanks FCT for the FCT Investigator starting grant IF/00973/2014.

References

- G. Hungerford, J. Benesch, J. F. Mano and R. L. Reis, *Photochem. Photobiol. Sci.*, 2007, **6**, 152–158.
- K. Kaur, R. Saini, A. Kumar, V. Luxami, N. Kaur, P. Singh and S. Kumar, *Coord. Chem. Rev.*, 2012, **256**, 1992–2028.
- X.-F. Zhang, J. Zhang and L. Liu, *J. Fluoresc.*, 2014, **24**, 819–826.
- R. Sjöback, J. Nygren and M. Kubista, *Spectrochim. Acta, Part A*, 1995, **51**, L7–L21.
- L. Zhang and X. Zhang, *Spectrochim. Acta, Part A*, 2014, **133**, 54–59.
- X.-F. Yang, Y. Li and Q. Bai, *Anal. Chim. Acta*, 2007, **584**, 95–100.
- E. Oliveira, J. Lorenzo, A. Cid, J. L. Capelo and C. Lodeiro, *J. Photochem. Photobiol., A*, 2013, **269**, 17–26.
- H. Zheng, X.-Q. Zhan, Q.-N. Bian and X.-J. Zhang, *Chem. Commun.*, 2013, **49**, 429–447.
- C. Lodeiro, J. L. Capelo, J. C. Mejuto, E. Oliveira, H. M. Santos, B. Pedras and C. Nuñez, *Chem. Soc. Rev.*, 2010, **39**, 2948.
- E. Oliveira, J. L. Capelo, J. C. Lima and C. Lodeiro, *Amino Acids*, 2012, **43**, 1779–1790.
- M. Mameli, V. Lippolis, C. Caltagirone, J. L. Capelo, O. N. Faza and C. Lodeiro, *Inorg. Chem.*, 2010, **49**, 8276–8286.
- H. N. Kim, W. X. Ren, J. S. Kim and J. Yoon, *Chem. Soc. Rev.*, 2012, **41**, 3210–3244.
- W.-Y. Liu, S.-L. Shen, H.-Y. Li, J.-Y. Miao and B.-X. Zhao, *Anal. Chim. Acta*, 2013, **791**, 65–71.
- D. W. Boening, *Chemosphere*, 2000, **40**, 1335–1351.
- J. Hu, J. Li, J. Qi and J. Chen, *New J. Chem.*, 2015, **39**, 843–848.
- S. Ekino, M. Susa, T. Ninomiya, K. Imamura and T. Kitamura, *J. Neurol. Sci.*, 2007, **262**, 131–144.
- C. Núñez, M. Diniz, A. a. Dos Santos, J. L. Capelo and C. Lodeiro, *Dyes Pigm.*, 2014, **101**, 156–163.
- W. Mertz, *J. Nutr.*, 1993, **123**, 626–633.
- K. N. Jeejeebhoy, *Nutr. Rev.*, 1999, **57**, 329–335.
- a. D. Dayan and a. J. Paine, *Hum. Exp. Toxicol.*, 2001, **20**, 439–451.
- B. Gordon, P. Callan and C. Vickers, *WHO Chron.*, 2008, **38**, 564.
- D. Krewski, R. a. Yokel, E. Nieboer, D. Borchelt, J. Cohen, J. Harry, S. Kacew, J. Lindsay, A. M. Mahfouz and V. Rondeau, *J. Toxicol. Environ. Health, Part B*, 2007, **10** (Suppl 1), 1–269.
- S. Han, J. Lemire, V. P. Appanna, C. Auger, Z. Castonguay and V. D. Appanna, *Cell Biol. Toxicol.*, 2013, **29**, 75–84.
- V. Rondeau, D. Commenges, H. Jacqmin-Gadda and J. F. Dartigues, *Am. J. Epidemiol.*, 2000, **152**, 59–66.
- B. Daly, J. Ling and a. P. de Silva, *Chem. Soc. Rev.*, 2015, **44**, 4203–4211.
- S. Das, M. Dutta and D. Das, *Anal. Methods*, 2013, **5**, 6262.
- J. Chan, S. C. Dodani and C. J. Chang, *Nat. Chem.*, 2012, **4**, 973–984.
- K. P. Carter, A. M. Young and A. E. Palmer, *Chem. Rev.*, 2014, **114**, 4564–4601.
- X. Li and J. S. Taylor, *Bioorg. Med. Chem.*, 2004, **12**, 545–552.
- A. Barba-bon, A. M. Costero, S. Gil, M. Parra and J. Soto, *Chem. Commun.*, 2012, **48**, 3000–3002.
- R. M. Silverstein, F. X. Webster and D. J. Kiemle, *Spectrometric identification of organic compounds*, John Wiley & Sons, Hoboken, 2005.
- J. Olmsted, *J. Phys. Chem.*, 1979, **83**, 2581–2584.
- T. Ueno, Y. Urano, K. I. Setsukinai, H. Takakusa, H. Kojima, K. Kikuchi, K. Ohkubo, S. Fukuzumi and T. Nagano, *J. Am. Chem. Soc.*, 2004, **126**, 14079–14085.
- T. Peng and D. Yang, *Org. Lett.*, 2010, **12**, 496–499.
- E. M. Nolan and S. J. Lippard, *Chem. Rev.*, 2008, **108**, 3443–3480.
- A. Tamayo, B. Pedras, C. Lodeiro, L. Escriche, J. Casabo, L. Capelo, B. Covelo, R. Kiveka and R. Sillanpa, *Inorg. Chem.*, 2007, **46**, 159–165.
- Y. Zhang, Y. Yang, J. Hao, C. Yin, F. Huo, J. Chao and D. Liu, *Spectrochim. Acta, Part A*, 2014, **132**, 27–31.
- Y. Yang, K. Yook and J. Tae, *J. Am. Chem. Soc.*, 2005, **1**, 16760–16761.
- G. Zhang, D. Zhang, S. Yin, X. Yang, Z. Shuai and D. Zhu, *Chem. Commun.*, 2005, **6**, 2161–2163.
- X. Guo, X. Qian and L. Jia, *J. Am. Chem. Soc.*, 2004, **126**, 2272–2273.
- G. Hennrich, W. Walther, U. Resch-genger and H. Sonnenschein, *Inorg. Chem.*, 2001, **40**, 641–644.
- Y. Zhao, Z. Lin, C. He, H. Wu and C. Duan, *Inorg. Chem.*, 2006, **45**, 10013–10015.
- H. Arakawa, R. Ahmad and M. Naoui, *J. Biol. Chem.*, 2000, **275**, 10150–10153.
- J. Ho Chang, Y. M. Choi and Y. K. Shin, *Bull. Korean Chem. Soc.*, 2001, **22**, 527–530.
- P. Gans, A. Sabatini and A. Vacca, *Talanta*, 1996, **43**, 1739–1753.
- F. Huo, Y. Sun, J. Su, Y. Yang and C. Yin, *Org. Lett.*, 2010, 1257–1260.
- N. Klonis and W. H. Sawyer, *Photochem. Photobiol.*, 2003, **77**, 502–509.
- B. Grzeszczyk, S. Stecko, Ł. Mucha, O. Staszewska-Krajewska, M. Chmielewski and B. Furman, *J. Antibiot.*, 2013, **66**, 161–163.
- M. Montalti, A. Credi, L. Prodi and M. T. Gandolfi, *Handbook of Photochemistry*, Taylor & Francis, Boca Raton, 3rd edn., 2006.